Measurement Science and Technology

PAPER • OPEN ACCESS

Far-field sectioning for the retrieval of subwavelength grating parameters using coherent Fourier scatterometry

To cite this article: Lauryna Siaudinyte and Silvania F Pereira 2020 *Meas. Sci. Technol.* **31** 104005

View the article online for updates and enhancements.

You may also like

- An insight into optical metrology in manufacturing
Yuki Shimizu, Liang-Chia Chen, Dae Wook Kim et al.

- Improved reconstruction of critical dimensions in extreme ultraviolet scatterometry by modeling systematic errors
Mark-Alexander Henn, Hermann Gross, Sebastian Heidenreich et al.

- Interferometric coherent Fourier scatterometry: a method for obtaining high sensitivity in the optical inverse-grating problem
S Roy, N Kumar, S F Pereira et al.

This content was downloaded from IP address 202.8.112.55 on 21/06/2023 at 05:32

OPEN ACCESS
IOP Publishing
Measurement Science and Technology
Meas. Sci. Technol. 31 (2020) 104005 (6pp)
https://doi.org/10.1088/1361-6501/ab7315

Far-field sectioning for the retrieval of subwavelength grating parameters using coherent Fourier scatterometry

Lauryna Siaudinyte and Silvania F Pereira

Faculty of Applied Sciences, Imaging Physics Department, Optics Research Group, Delft University of Technology, Lorentzweg 1, 2628CJ Delft, The Netherlands

E-mail: L.Siaudinyte@tudelft.nl

Received 29 November 2019, revised 21 January 2020
Accepted for publication 5 February 2020
Published 13 July 2020

Abstract

Optical inspection of periodic nanostructures is a major challenge in the semiconductor industry due to constantly decreasing critical dimensions. In this paper we combine coherent Fourier scatterometry (CFS) with a sectioning mask for subwavelength grating parameter determination. By selecting only the most sensitive regions of the scattered light in the Fourier plane, one can retrieve grating parameters faster and with higher sensitivity than previous approaches. Moreover, the full process of CFS using focused light is explained and implemented in a subwavelength grating regime. The results of using transverse magnetic polarized input fields together with the proposed sectioning mask are presented and compared to the non-mask case.

Keywords coherent Fourier scatterometry, beam shaping, diffraction, scattered light, grating, periodic nanostructure, optical inspection

(Some figures may appear in colour only in the online journal)

1. Introduction

Optical scatterometry is a very commonly used measurement technique in the fields of photonics, optics, electronics, biology, and medicine, where non-destructive measurement methods are required [1,2]. In the semiconductor industry, there is a huge demand for the manufacture of periodic nanostructures in order to implement them in electronic circuits. Therefore, constant development of advanced non-contact optical measurement methods, configurations and sensitivity analyses is essential in order to inspect the geometrical properties of these nanostructures as well as their surface quality [3–7]. Recently, attention has been directed towards coherent Fourier scatterometry (CFS) which in a prior study [8] was reported as a method offering smaller uncertainty and higher sensitivity to the changes of grating geometrical parameters in comparison to incoherent Fourier scatterometry (IFS). Due to the continuously shrinking size of microelectronic components, the scale of periodic nanostructures is decreasing accordingly. Therefore, there is a need for further research on the subwavelength grating regime. In recent approaches [9] it was reported that, by imaging the target through multiple focus positions, it is possible to reconstruct the scattered volume. Therefore, this method can be applied for the determination of the parameters of nanostructures. Another method using white light interference Fourier scatterometry has been successfully implemented and used in practice [10]. CFS is based on focusing coherent light on a structure and collecting the light in reflection within the numerical aperture of a focusing objective. After interaction with the sample, the light in the back focal plane (Fourier plane) is imaged by a CCD camera [3]. In this way, the scattered light at all angles is obtained in one shot [8]. The structure is characterized based on the unique intensity pattern captured in the back focal plane, and in the case of subwavelength grating, without scanning. This far-field intensity pattern contains the information about the

Original content from this work may be used under the terms of the Creative Commons Attribution 4.0 licence. Any further distribution of this work must maintain attribution to the author(s) and the title of the work, journal citation and DOI.

 © 2020 The Author(s). Published by IOP Publishing Ltd Printed in the UK

grating's geometrical parameters as well as its surface. In order to retrieve the parameters of the grating under test, it is useful to perform a sensitivity analysis to determine the influence of the input parameters on the simulation results [11]. The precision of the retrieval of the sample's parameters increases with the higher sensitivity to the change of these parameters. Sensitivity is determined by analysing changes caused by modified parameter values in the intensity pattern [12]. Depending on the input field and the sample surface, the sensitivity is usually uneven throughout the pupil plane. Moreover, generating simulations of intensity patterns within the full aperture of the pupil is time consuming [13].

Therefore, the goal of this research is to determine the most sensitive segments of the complex scattered field and to use them for more efficient retrieval of subwavelength grating parameters.

In this paper, we propose a sectioning mask which will help to analyse only the most sensitive segments of the light patterns in a Fourier plane. In this way, due to data reduction it becomes a time saving tool for the retrieval of subwavelength grating parameters.

Polarization of light is also an important variable in scatterometry. Depending on the sample material, shape of the structure and wavelength used , the use of different polarisation states might influence the measurement results significantly [14]. Silicon in the semiconductor industry is very valuable due to its thermal stability and resistance to other environmental conditions [15]. Therefore, for this research a 1D silicon-on-silicon grating is used as a sample together with transverse magnetically (TM) polarized light in the subwavelength regime. These gratings are widely used in the fabrication of microchips and other electronic components.

2. Coherent Fourier scatterometry and the experimental setup

During the experiment, coherent light of 633 nm wavelength emitted from a He-Ne laser was coupled to a single-mode fibre and further collimated by a lens. As is shown in the scheme of the experimental setup (figure 1), the incoming light was directed to the polarizer which determined the polarization direction of the input field (either transverse electric (TE) or transverse magnetic (TM), i.e. parallel or perpendicular to the grating lines). After passing through the polarizer and the beam splitter, the light reached the microscope objective, where it was focused on the sample containing a subwavelength silicon-on-silicon grating.

After reflection, the light travelled back through the same objective, and its back focal plane was imaged by the CCD camera, where the 2D intensity distribution of the far field was obtained. Before reaching the CCD camera, the light passed through another polarizer which determined the polarization (TE or TM) of the output field. In this way, all relevant combinations of input-output polarizations can be obtained: TE-TE, TE-TM, TM-TM, and TM-TE. With the addition of one lens, one can obtain the phase distribution of the far field using phase retrieval techniques [16].

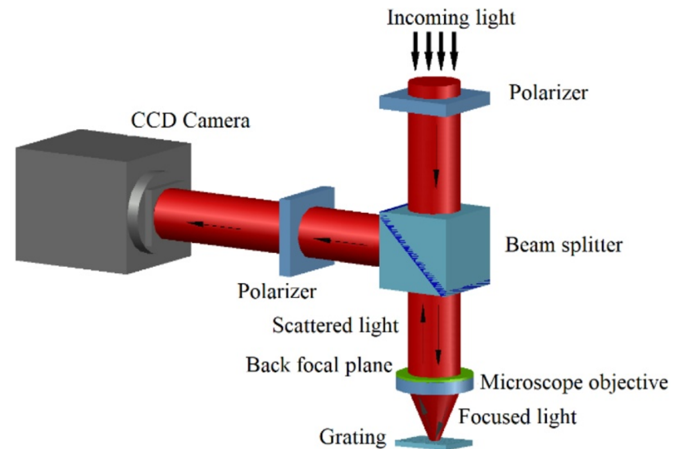

Figure 1. Scheme of the coherent Fourier scatterometry (CFS) setup for retrieval of geometrical.

grating parameters.

In the arrangement shown in figure 1, the focused light is understood as multiple plane waves pointed at the same spot with different angles of incidence, as described similarly in [17]. After the interaction with the grating, the reflected fields corresponding to all the incoming plane waves add up coherently and create the far-field intensity pattern which is recorded by the CCD camera.

Scatterometry is based on a comparison of the measured and the simulated electromagnetic field distribution in the far field. In order to obtain realistic simulations, it is necessary to measure the properties of the incoming light. The incident electromagnetic field was measured by a wavefront sensor based on the Shack–Hartmann principle. This is a traditional, commercially available and one of the most commonly used sensors to obtain the wavefront of a light beam [18]. Further, it is essential to have *a priori* knowledge about the sample. For this, we used the nominal grating parameters: height (h) = 130 nm, grating pitch (d) = 500 nm, sidewall angle (SWA) = 90°, middle linewidth of critical dimension (midCD) = 216 nm. Also, we chose to analyse the TMTM case, in which both the incoming and outgoing light had TM polarization, because the far field in this case was richer than other polarisation combinations. The numerical aperture of the system was 0.4.

3. Computational modelling and results

3.1. Sensitivity determination in the far field

In order to analyse the most sensitive regions of the far field, computational simulations were performed by using rigorous coupled-wave analysis (RCWA) which solves Maxwell's equations based on periodic conditions and computes the efficiency of the diffraction orders in the far field for each incident angle on the grating.

Far-field intensity distributions captured in the Fourier plane (figure 2) were generated based on the aforementioned nominal parameters and used as a reference for other far fields,

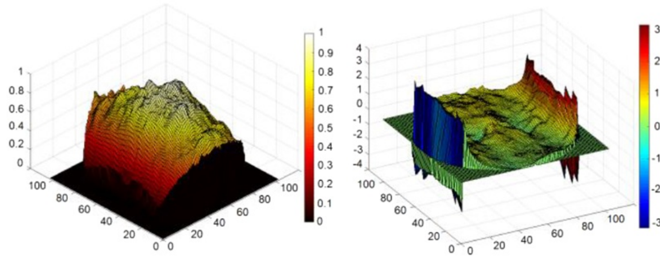

Figure 2. Simulated nominal parameter-based far fields within the numerical aperture: amplitude (left) and phase (right). Axes are given in pixels, and are bounded by the numerical aperture of the system.

which were computed by applying other grating heights and sidewall angle combinations. Each point in figure 2 represents one scattering angle and the position (location) within the numerical aperture of the system.

To analyse the sensitive regions of the far field, scatterograms covering parameter combinations of changes in the grating height ±10 nm (120 nm–140 nm) and the sidewall angle ±5° (80°–90°) were created. The sensitive regions of all combinations can be simply determined by analysing differences between the far field based on the nominal grating parameters and the simulated far field with certain combinations of grating geometrical parameters. The quantification of such a difference (equation (1)) is based on a sum of squared difference between the matrix A_{nom} generated with nominal grating parameters and the estimated matrix A_{est} which is generated by changing one or both parameters (grating height and sidewall angle). For a clear visualization, it is convenient to normalize the data according to a matrix based on nominal parameters. Therefore, the sensitivity to a minor parameter change could be expressed as follows:

$$\Delta = \frac{\int \sqrt{|A_{est}(x,y) - A_{nom}(x,y)|^2} dxdy}{\int \sqrt{|A_{nom}(x,y)|^2} dxdy}. \quad (1)$$

Equation (1) lets us quantify and evaluate the amplitude- or phase input-based pattern in the far field pixel by pixel. For comparison with experimental data, presented further in this paper, the CCD camera pixels' values of the far-field image were interpolated and digitized to match the number of pixels of the computed far fields. For the simulations a matrix of 103 × 103 values was used to visualize the scattered light in the Fourier plane.

Differences of the intensity and phase patterns between the far field simulated by using nominal grating parameters and far fields simulated by using various other combinations of grating height and sidewall angle have been simulated. In figures 3 and 4, we show these differences of the intensity and phase patterns for a few cases of sidewall angle (SWA) and height combinations, as indicated on top of each subfigure. Note that, for some parameter combinations, the differences are bigger in certain regions of the pupil.

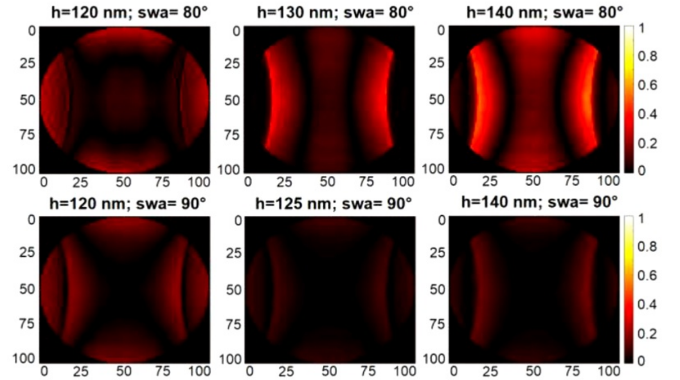

Figure 3. Normalized sensitivity maps for some grating height and sidewall angle combinations for the amplitude of the scattered field.

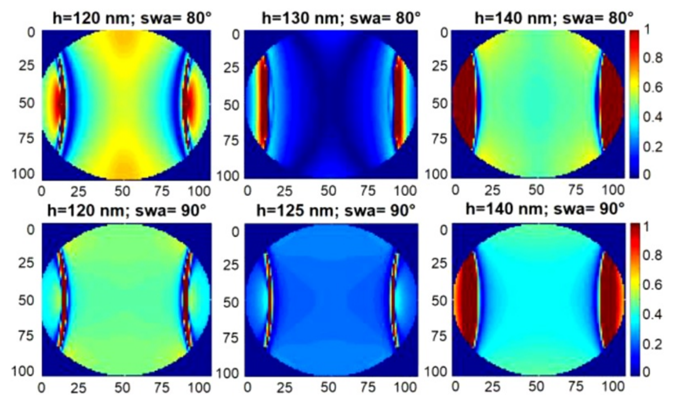

Figure 4. Normalized sensitivity maps for some grating height and sidewall angle combinations for the phase of the scattered field.

The values of height and sidewall angle are indicated on the top of each subfigure. The limits of the plots represents the numerical aperture of the system.

3.2. Sectioning of the pupil plane

RCWA is an efficient tool in scatterometry for solving Maxwell's equations, dealing with the inverse problem of scatterometry and computing the electromagnetic far field. For CFS one has to implement the calculations for all incident angles within the numerical aperture of the optical system and sum them coherently to obtain the full far field. Although the calculation speed is sufficient, in terms of sensitivity quantification, considering the entire pupil with all insensitive regions is not the best option. Therefore, we propose to isolate only the most sensitive areas of the pupil.

After generating intensity patterns for various height and sidewall angle combinations, it turned out that the sensitive regions differ depending on whether the amplitude or phase data are considered. Therefore, it was decided to apply different sectioning masks for phase- and amplitude-based far fields.

As is shown in figure 5, the segments of the sectioning mask cover only the part of the most sensitive regions. Both the size and the position of the sectioning mask were optimized to fit

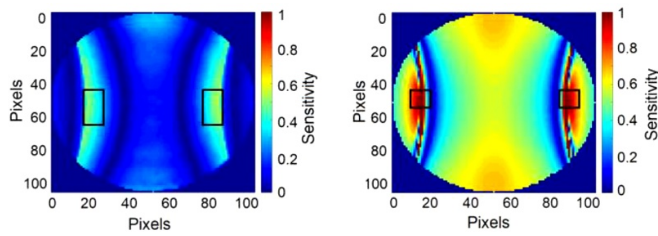

Figure 5. Sectioning mask for the amplitude (left) and the phase (right) based far fields.

the far-field simulations of various sidewall angle and height combinations.

The mask was designed to cover a sufficient part of the sensitive region and was chosen after comparing different sizes of the masks in different locations of the sensitive regions. The size of the mask for the amplitude was 10 × 20 pixels and for the phase 10 × 10 pixels due to the narrower sensitivity region. The bigger mask size in this case would have included information of the insensitive area and the smaller mask would have covered only very few angles of incidence, which would not have been sufficient to collect the necessary information about the grating.

After selecting the previously mentioned segments, the sensitivity quantification procedure was repeated in order to verify the efficacy of the proposed sectioning mask. Also, it is important to note, that after the application of the sectioning mask the computational modeling time decreased 10–15 times due to the smaller amount of data.

The results showed that application of the sectioning mask increased sensitivity by 3 times for the amplitude and 1.2 times for the phase, as presented in figure 6. This figure represents the normalized sensitivity of the computed far fields in arbitrary units for every height and sidewall angle combination of the subwavelength grating. The use of the phase of the far field provides higher sensitivity than the amplitude counterpart. However, it is more difficult to measure the phase after interaction with the sample compared to the amplitude. Depending on the polarization, a Shack–Hartmann wavefront sensor is not an option since the far field has phase jumps. This was the case for our grating under test with TM-TM input-output polarization. Thus, in this situation, other methods such as interferometry or phase retrieval should be used. Since the sensitivity based on the far-field amplitude increases significantly after sectioning, it could be sufficient to use only amplitude measurements for the retrieval of grating parameters and set the complicated phase measurement procedure aside.

3.3. Comparison of measured and simulated electromagnetic fields

In order to fully realize the concept of scatterometry, the electromagnetic field measured after the interaction with the sample has to be compared with the simulated electromagnetic field. For this part of the experiment, all the computed far fields with different combinations of grating height and sidewall angle around the nominal parameters were compared with the measured amplitudes of the scattered field for the case of the full pupil and the sectioning mask (as indicated in figure 5). The results obtained by using the amplitude of the far field are shown in figure 7.

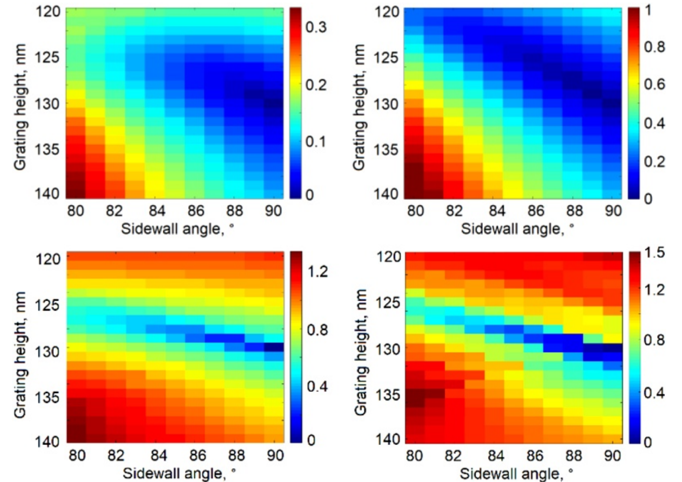

Figure 6. Sensitivity of the simulated far fields before (left) and after (right) applying the sectioning mask. Top maps: Amplitude; bottom maps: phase.

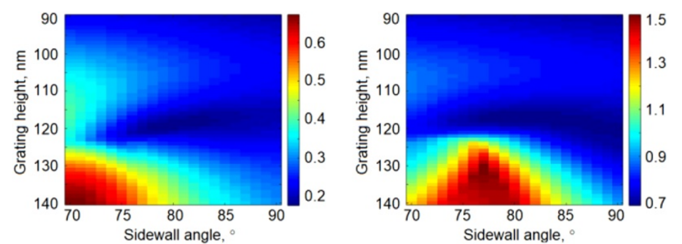

Figure 7. Comparison of the reconstruction error between the measured and the simulated far-field amplitude for the full pupil (left) and the sectioning mask (right).

Since both approaches (with and without the sectioning mask) showed the smallest difference between simulated and measured electromagnetic fields when the sidewall angle of the grating was 80°, it was decided to analyze this segment with a fixed sidewall angle and changing grating height.

The comparison displayed in figure 8 reveals that by applying the proposed sectioning mask, the parameters of the subwavelength grating can be determined with higher precision since the transition between the values is steeper (sharper) compared to the values within the full pupil. The reconstructed grating height was 117 nm with sectioning mask and 119 nm without sectioning mask. However, the mismatch between the measured and the simulated electromagnetic fields is bigger after the sectioning. Since these sections are the most sensitive in the entire pupil, due to the smaller intensity of the light, they contain a higher noise level. In order to increase the signal-to-noise ratio, the setup could be improved by enhancing the light intensity within the sectioning mask.

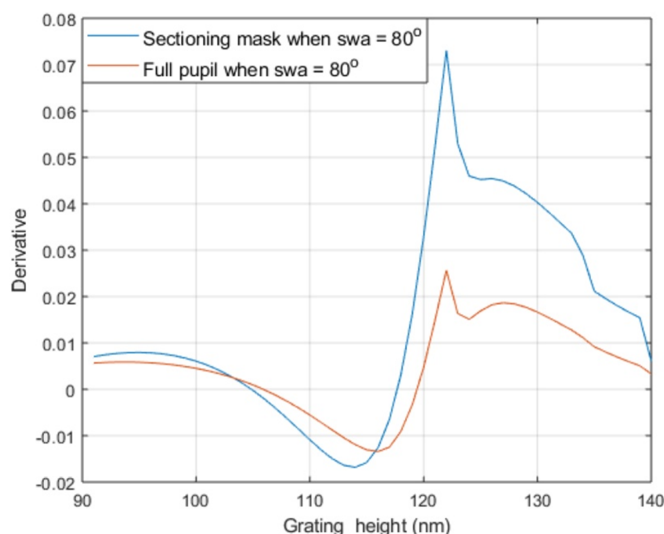

Figure 8. Derivatives of the reconstruction error of the sectioning mask and the full pupil when the sidewall angle is fixed at 80°.

4. Discussion

In order to check the real parameters of the grating, it is recommended to perform additional independent measurements, i.e. by using 3D atomic force microscopy. Also, it is important to mention that, in our simulations, the oxide layer covering the sample was not considered. The oxide layer was measured by ellipsometry and the determined thickness was 7.2 nm. The literature suggests that the oxide layer can affect the reconstruction of grating parameters such as height, midCD and SWA [19]. Moreover, the oxide layer was thicker than expected and might have contained not only the native oxide layer but also fabrication residuals with a similar refractive index as the oxide layer. We believe that the oxide layer is one of the reasons for the mismatch between the nominal and reconstructed grating height and sidewall angle. Another important aspect lies in our available implementation of the rigorous coupled-wave analysis (RCWA) algorithm, where the rounding of the grating line corners is not considered — this can also cause inaccuracies in the calculation of the far field. In order to increase the accuracy of the retrieval of grating parameters, our model will be improved by more diligent implementation of RCWA or by finite element method-based algorithms, as well as taking into consideration additional parameters such as top and bottom corner roundings of the grating line and the oxide layer, similarly as described in [20–22].

5. Conclusions

The research carried out and presented in this paper shows coherent Fourier scatterometry with a focused light used for subwavelength gratings. We presented an analysis of the effect of sectioning the far field in order to isolate the most sensitive regions, as the height and sidewall angle parameters were varied. The complex electromagnetic fields in the Fourier plane were simulated for grating height (ranging from 90 nm to 140 nm) and sidewall angle (ranging from 70° to 90°) combinations. After analysing the sensitivity of the amplitude and the phase in the far field, it was observed that the sensitive regions in both cases are not the same. Moreover, a comparison of numerical simulations with the experimentally measured data of both cases (full pupil vs sections) showed the advantage of far-field sectioning.

Sectioning masks, by which only the most sensitive segments of the pupil are used to determine the parameters of subwavelength gratings, were proposed. Application of the sectioning mask resulted in a method offering higher sensitivity, higher speed and less data storage consumption compared to former approaches which used the full far-field map [13]. However, because of the low signal-to-noise ratio in the sensitive regions, the precision of the retrieved grating parameters was low, and, therefore, the data could be improved by increasing the light intensity within the sensitive regions.

Acknowledgements

This project received funding from the European Union's Horizon 2020 research and innovation programme under the Marie Skłodowska-Curie grant agreement No. 707404. The opinions expressed in this document reflect only the authors' view. The European Commission is not responsible for any use that may be made of the information it contains. We would like to thank Dr Iman Zadeh for helping with the ellipsometry measurements of the oxide layer.

ORCID iD

Lauryna Siaudinyte https://orcid.org/0000-0003-1214-6552

References

[1] Krauter J, Gronle M and Osten W 2017 Optical inspection of hidden MEMS structures *Proc. SPIE* **10329** 1032914
[2] Turzhitsky V, Qiu L, Itzkan I, Novikov A, Kotelev M, Getmanskiy M, Vinokurov V, Muradov A and Pelerman L 2004 Spectroscopy of scattered light for the characterization of micro and nanoscale objects in biology and medicine *Appl. Spectrosc.* **68** 2
[3] El Gawhary O, Kumar N, Pereira S and Coene W 2011 Performance analysis of coherent Fourier scatterometry *Appl. Phys.* **105** 4
[4] Constantoudis V, Papavieros G, Lorusso G, Rutigliani V, Roey F and Gogolides E 2018 Computational nanometrology of line-edge roughness: noise effects, cross-line correlations and the role of etch transfer *Proc. SPIE* **10589** 105890Y
[5] Madsen M and Hansen P 2016 Scatterometry—fast and robust measurements of nano-textured surfaces *Surf. Topogr. Metrol. Prop.* **4** 023003
[6] Dong Z, Liu S, Chen X and Zhang C 2014 Determination of an optimal measurement configuration in optical scatterometry using global sensitivity analysis *Thin Solid Films* **562** 16–23
[7] Chen X, Liu X, Zhang C and Jiang H 2013 Measurement configuration optimization for grating reconstruction by Mueller matrix polarimetry *J. Micro/Nanolith. MEMS MOEMS* **12** 033013

[8] Kumar N, Petrik P, Ramanandran G, Gawhary O, Roy S, Pereira S, Coene W and Urbach P 2014 Reconstruction of sub-wavelength features and nano-positioning of gratings using coherent Fourier scatterometry *Opt. Express* **22** 24678
[9] Qin J, Silver R, Barnes B, Zhou H, Dixson R and Henn M 2016 Deep subwavelength nanometric image reconstruction using Fourier domain optical normalization *Light. Sci. Appl.* **5** e16038
[10] Paz V, Peterhansel S, Frenner K and Osten W 2012 Solving the inverse grating problem by white light interference Fourier scatterometry *Light. Sci. Appl.* **1** e36
[11] Farchmin N, Hammerschmidt M, Schneider P, Wurm M, Bodermann B, Bär M and Heidenreich S 2019 Efficient global sensitivity analysis for silicon line gratings using polynomial chaos *Proc. SPIE* **11057** https://doi.org/10.1117/12.2525978
[12] Littau M, Forman D, Bruce J, Raymond C H and Hummel S 2006 Diffraction signature analysis methods for improving scatterometry precision *Proc. SPIE* **6152**
[13] Kumar N, Cisotto L, Roy S, Ramanandan G, Pereira S F and Urbach H P 2016 Determination of the full scattering matrix using coherent Fourier scatterometry *Appl. Opt.* **55** 16
[14] EE H, Kang J, Brongersma M and Seo M 2015 Shape-dependent light scattering properties of subwavelength silicon nanoblocks *Nano Lett.* **15**
[15] Kroker S, Käsebier T, Steiner S, Kley E and Tünnermann A 2013 High efficiency two-dimensional grating reflectors with angularly tunable polarization efficiency *Appl. Phys. Lett.* **102** 161111
[16] Xu X, Konijnenberg A, Pereira S and Urbach P 2017 Phase retrieval of the full vectorial field applied to Coherent Fourier scatterometry *Opt. Express* **25** 29574
[17] Brown T, Alonso M, Vella A, Theisen M, Head S, Gillmer S and Ellis J 2014 Focused beam scatterometry for deep subwavelength metrology *Proc. Three-Dimensional and Multidimensional Microscopy: Image Acquisition and Processing XXI* **8949**
[18] Wu Y, Sharma M and Veeraraghavan A 2019 WISH: wavefront imaging sensor with high resolution *Light. Sci. Appl.* **8** 44
[19] Endres J, Kumar N, Petrik P, Henn M A, Heidenreich S, Pereira S F, Urbach P and Bodermann B 2014 Measurement comparison of goniometric scatterometry and coherent Fourier scatterometry *Proc SPIE* **9132** https://doi.org/10.1117/12.2052819
[20] Wurm M, Endres J, Probst J, Schoengen M, Diener A and Bodermann B 2017 Metrology of nanoscale grating structures by UV scatterometry *Opt. Express* **25** 3
[21] Gushchin I and Tishchenko A 2010 Fourier modal method for relief gratings with oblique boundary conditions *J. Opt. Soc. Am.* **27**
[22] Popov E, Neviere M, Gralak B and Tayeb G 2002 Staircase approximation validity for arbitrary-shaped gratings *J. Opt. Soc. Am.* **19**